Effect of spin excitations with simultaneous magnetic- and electric-dipole character on the static magnetoelectric properties of multiferroic materials

Dávid Szaller,[1] Sándor Bordács,[2] Vilmos Kocsis,[1] Toomas Rõõm,[3] Urmas Nagel,[3] and István Kézsmárki[1,4]
[1]*Department of Physics, Budapest University of Technology and Economics, 1111 Budapest, Hungary*
[2]*Quantum-Phase Electronics Center, Department of Applied Physics, The University of Tokyo, Tokyo 113-8656, Japan*
[3]*National Institute of Chemical Physics and Biophysics, Akadeemia tee 23, 12618 Tallinn, Estonia*
[4]*MTA-BME Condensed Matter Research Group, 1111 Budapest, Hungary*
(Received 13 January 2014; revised manuscript received 28 April 2014; published 27 May 2014)

We derive a sum rule to demonstrate that the static magnetoelectric (ME) effect is governed by optical transitions that are simultaneously excited by the electric and magnetic components of light. The ME sum rule is applicable to a broad class of materials lacking the spatial inversion and the time-reversal symmetries, including multiferroic compounds. Due to the dynamical ME effect, the optical excitations in these materials can exhibit directional dichroism, i.e., the absorption coefficient can be different for counter-propagating light beams. According to the ME sum rule, the magnitude of the linear ME effect of a material is mainly determined by the directional dichroism of its low-energy optical excitations. An application of the sum rule to the multiferroic $Ba_2CoGe_2O_7$, $Sr_2CoSi_2O_7$, and $Ca_2CoSi_2O_7$ shows that in these compounds the static ME effect is mostly governed by the directional dichroism of the spin-wave excitations in the giga-terahertz spectral range. On this basis, we argue that the studies of directional dichroism and the application of the ME sum rule promote the synthesis of new materials with large static ME effect.

DOI: 10.1103/PhysRevB.89.184419 PACS number(s): 76.50.+g, 75.85.+t, 78.20.Ls

I. INTRODUCTION

Magnetoelectric (ME) multiferroics, where ferroelectricity coexists with (ferro)magnetism, represent the most extensively studied class of multiferroics [1–6]. A spectacular control of the ferroelectric polarization by magnetic field and manipulation of the magnetic order via electric field can be realized in most of these materials as a direct consequence of the coupling between spins and local electric dipoles. This offers a fundamentally new path for data storage by combining the best qualities of ferroelectric and magnetoresistive memories: fast low-power electrical write operation, and nondestructive nonvolatile magnetic read operation [5,6]. The efficiency of multiferroics in such memory applications depends on the strength of the magnetization-polarization coupling responsible for the ME phenomena.

The ME effect has also been proposed to open new perspectives in photonics. The entanglement between spins and local polarization governs not only the ground-state properties but also the character of excited states. Consequently, the electric component of light induces precession of the spins and the magnetic component of light generates electric polarization waves. This is termed as the optical ME effect and has recently been observed for the spin excitations in several multiferroic compounds [7–15].

As one of the most peculiar manifestations of the ME effect in the optical regime, counter-propagating light beams can experience different refractive indices. Indeed, strong directional dichroism, that is difference in the absorption coefficient for light beams traveling in opposite directions, has been reported for spin excitations in multiferroics and proposed as a new principle to design directional light switches operating in the giga-terahertz (GHz-THz) region [10–14].

Here, we show that optical studies of low energy magnons in ME multiferroics provide an efficient tool to further elucidate microscopic mechanisms of multiferroicity. These studies can be particularly useful to promote the systematic synthesis of new materials with large static ME effect. We derive a relation, hereafter referred to as the *ME sum rule*, which shows the connection between the static ME effect and the directional dichroism observed for low-energy excitations. We demonstrate the applicability of the ME sum rule for three multiferroic materials, $Ba_2CoGe_2O_7$ (BCGO), $Sr_2CoSi_2O_7$ (SCSO), and $Ca_2CoSi_2O_7$ (CCSO), by comparing their directional dichroism spectra to the corresponding static ME coefficients reported in the literature [16–21]. The absorption measurements used to determine the directional dichroism in the GHz-THz spectral range were performed in the present study and partly reproduced from our former works [10–12].

The Kramers-Kronig relation, also known as the Hilbert transformation, connects the real ($\Re$) and imaginary ($\Im$) parts of a general frequency dependent susceptibility $\chi(\omega)$, which corresponds to a linear and causal response function in the time domain:

$$\Re\chi(\omega) = \frac{1}{\pi}\mathcal{P}\int_{-\infty}^{\infty}\frac{\Im\chi(\omega')}{\omega'-\omega}\mathrm{d}\omega',$$

$$\Im\chi(\omega) = -\frac{1}{\pi}\mathcal{P}\int_{-\infty}^{\infty}\frac{\Re\chi(\omega')}{\omega'-\omega}\mathrm{d}\omega',$$

where $\mathcal{P}$ stands for the Cauchy principal value integral. In many cases, either the real or the imaginary part of $\chi(\omega)$ can be determined experimentally and the Kramers-Kronig transformation is used to obtain the entire complex response function. In the limit of $\omega \to 0$, these expressions are simplified to the following form, which shows close similarity with sum rules,

$$\Re\chi(\omega=0) \equiv \chi(0) = \frac{2}{\pi}\mathcal{P}\int_{0}^{\infty}\frac{\Im\chi(\omega)}{\omega}\mathrm{d}\omega, \quad (1)$$

$$\Im\chi(\omega=0) \equiv 0 = -\frac{1}{\pi}\mathcal{P}\int_{-\infty}^{\infty}\frac{\Re\chi(\omega)}{\omega}\mathrm{d}\omega. \quad (2)$$

Equation (1) shows that the static response of a system is fully determined by the corresponding dynamical susceptibility and the frequency denominator on the right-hand side indicates the vital role of low-energy excitations in the static susceptibility.

A common example is the dielectric permittivity of semiconductors, which is usually larger for compounds with smaller charge gap and can be considerably affected by the contributions from low-energy phonon modes. A particularly strong enhancement of the dielectric permittivity is found in quantum paraelectrics due to the presence of soft polar phonon modes [22,23]. The domain wall dynamics can also influence the static response in materials with ferroic orders.

In multiferroic materials, the coupling between the electric polarization and the magnetization can be phenomenologically described by the ME susceptibility tensors $\chi^{me}(\omega)$ and $\chi^{em}(\omega)$, where $\Delta M^{\omega}_{\gamma} = (\varepsilon_0/\mu_0)^{1/2}\chi^{me}_{\gamma\delta}(\omega)E^{\omega}_{\delta}$ is the magnetization generated by an oscillating electric field and $\Delta P^{\omega}_{\delta} = c^{-1}\chi^{em}_{\delta\gamma}(\omega)H^{\omega}_{\gamma}$ is the polarization induced by an oscillating magnetic field. Here, ε_0 and μ_0 are the vacuum permittivity and permeability, respectively, and c is the speed of light in vacuum, while γ and δ stand for the Cartesian coordinates. The two cross-coupling tensors are connected by the time-reversal operation $\{\ldots\}'$ according to $\{\chi^{me}_{\gamma\delta}(\omega)\}' = -\chi^{em}_{\delta\gamma}(\omega)$. Although the static ME susceptibility $\chi^{me}_{\gamma\delta}(0)$ is always antisymmetric with respect to the time reversal (time-reversal odd), this is not true for the dynamical ME effect. In fact, the time-reversal even parts of the diagonal $\chi^{me}_{\gamma\gamma}(\omega \neq 0)$ tensor elements are responsible for the natural optical activity in chiral materials [24,25]. Recently, manifestations of magnetically induced chirality have been observed at spin excitations of multiferroic BCGO [11].

A broad class of materials simultaneously lacking the spatial inversion and the time-reversal symmetries [26–31], including multiferroics, can differentiate between counter-propagating electromagnetic waves since the time-reversal odd part of the ME susceptibility appears as a nonreciprocal term in their refractive indices. However, it is hard to derive the exact form of the refractive index for most of these materials due to their low symmetries. Moreover, the propagating solutions of the Maxwell equations are usually elliptically polarized waves in these systems. Nevertheless, when measuring the transmission of a sufficiently thin sample with linearly polarized light, the polarization of light is nearly preserved during propagation through the specimen and the index of refraction has a simple form [10–12,30,32,33]

$$N^{\pm}(\omega) \approx \sqrt{\varepsilon_{\delta\delta}(\omega)\mu_{\gamma\gamma}(\omega)} \pm \tfrac{1}{2}\left[\chi^{me}_{\gamma\delta}(\omega) - \{\chi^{me}_{\gamma\delta}(\omega)\}'\right], \quad (3)$$

where $N^{\pm}$ stands for the refractive indices of waves propagating in opposite directions ($\pm\boldsymbol{k}$). The δ and γ coordinate axes are parallel to the direction of the electric ($\mathbf{E}^{\omega}$) and magnetic ($\mathbf{H}^{\omega}$) fields of light, respectively, while $\varepsilon_{\delta\delta}(\omega)$ and $\mu_{\gamma\gamma}(\omega)$ are diagonal components of the dielectric permittivity and the magnetic permeability tensors. In some special cases, the exact solutions of Maxwell's equations are given in the literature where the propagating solutions are either linearly or circularly polarized waves [12].

The difference in the imaginary part of the N^{+} and N^{-} refractive indices in Eq. (3) gives rise to a difference in the absorption coefficients of counter-propagating waves, termed as directional dichroism:

$$\Delta\alpha(\omega) = \alpha_{+}(\omega) - \alpha_{-}(\omega) = \frac{2\omega}{c}\Im\left[\chi^{me}_{\gamma\delta}(\omega) - \left\{\chi^{me}_{\gamma\delta}(\omega)\right\}'\right]. \quad (4)$$

This relation between the directional dichroism $\Delta\alpha$ and ME susceptibilities is valid whenever Eq. (3) is valid, it is if the linear polarization of light is preserved during the propagation through the ME medium. We show in Appendix A that Eq. (3) can even be applied for materials where the solutions of the Maxwell equations are circularly polarized waves if a polarization-independent detection scheme is used.

As another approximation in Eq. (3), we neglect the longitudinal component of the polarization induced, e.g., by magnetization perpendicular to the light propagation. Thus we neglect additional terms in the refractive index, which are higher-order products of off-diagonal tensor components like $\chi^{me}_{\delta\beta}\epsilon_{\beta\gamma}/\epsilon_{\beta\beta}$ or $\chi^{me}_{\beta\delta}\mu_{\beta\gamma}/\mu_{\beta\beta}$; here, β denotes the axis of the light propagation.

II. RESULTS

A. The ME sum rule

Application of the Kramers-Kronig relations to the linear ME susceptibility gives rise to sum rules analogous to Eqs. (1) and (2). The main fundamental difficulty with the application of these sum rules is that usually $\chi^{me}(\omega)$ cannot be determined from the optical quantities of the material, since different contributions to the refractive index coming from the dielectric permittivity, the magnetic permeability and the ME susceptibility can hardly be separated. Consequently, in their generally valid forms Eqs. (1) and (2) have little practical use for the ME response.

However, using Eq. (4), the general sum rule in Eq. (1) can be reformulated in a more specific way, which directly connects the static ME effect to the directional dichroism spectrum:

$$\chi^{me}_{\gamma\delta}(0) = \frac{c}{2\pi}\mathcal{P}\int_0^{\infty}\frac{\Delta\alpha(\omega)}{\omega^2}\mathrm{d}\omega. \quad (5)$$

According to this sum rule the static ME effect is mostly governed by the directional dichroism of low-energy excitations, since the absorption difference, $\Delta\alpha$, is cut off by the ω^2 denominator at higher frequencies.

In Appendix B, we derive the same ME sum rule using the Kubo formula and show that only the time-reversal odd parts of the off-diagonal elements in $\chi^{me}(\omega)$ can contribute to the integral in Eq. (1). Thus the dynamical ME susceptibility in the sum rule can be replaced by the directional absorption difference according to Eq. (4). It also means that the ME sum rule in Eq. (5) is applicable for all materials where there are finite off-diagonal elements in the static ME tensor [34]. The special conditions to observe directional dichroism in these materials are discussed in details in Ref. [26].

A similar sum rule was recently developed for ME media by generalizing the Lyddane-Sachs-Teller relation [35]. However, its applicability to multiferroic materials with low symmetry is again limited because it requires the experimental determination of all elements of the ME tensor.

B. Application of the ME sum rule to multiferroic materials

In order to verify the applicability of the ME sum rule, we compare the magnetic field dependence of the static and optical ME effects for three members of the multiferroic melilite family, namely for $Ba_2CoGe_2O_7$, $Ca_2CoSi_2O_7$, and $Sr_2CoSi_2O_7$. These compounds crystallize in the noncentrosymmetric tetragonal $P\bar{4}2_1m$ structure [36–39] where Co^{2+} cations with $S = 3/2$ spins form square-lattice layers stacked along the tetragonal [001] axis. They undergo an antiferromagnetic transition at $T_N \approx 6$–7 K. Due to strong single-ion anisotropy, the two-sublattice antiferromagnetic state has an easy-plane character with spins lying within the tetragonal plane [20,38,40–42]. The free rotation of the magnetization within the tetragonal plane can already be realized by moderate fields of $\lesssim$1–2 T, which is an indication of a weak in-plane anisotropy [18,43]. As another consequence of the single-ion anisotropy, the magnetization is saturated at different magnetic field values, $H^{\rm Sat}_{\rm plane}$ and $H^{\rm Sat}_{\rm axis}$, when the field is applied within the easy plane or along the hard axis. Prior to saturation the magnetization follows a nearly linear field dependence due to the increasing canting of the sublattice moments for any direction of the magnetic field.

The ME properties of these materials have been studied extensively theoretically [44–46] and experimentally [16–20,40,47]. The strong optical ME effect emerging at their spin-wave excitations has also attracted much interest [10–12,32,33,48,49]. The magnetically induced ferroelectric polarization originates from the spin-dependent hybridization of the Co^{2+} d orbitals with the p orbitals of the oxygen ions forming tetrahedral cages around the Co spins [18,19]. When the magnetization is a linear function of the applied field, the direction of the sublattice magnetizations can be straightforwardly expressed as a function of the orientation and the magnitude of the magnetic field. Then, within the spin dependent hybridization model, the ferroelectric polarization is determined by the orientation of sublattice magnetizations [18,50]:

$$P_{[100]} = A_p\left[h_p \sin\theta - \sqrt{1-(h_p\sin\theta)^2}\right] \times \sqrt{1-(h_a\cos\theta)^2}\, h_a \cos\theta \sin\phi, \quad (6)$$

$$P_{[010]} = A_p\left[h_p \sin\theta - \sqrt{1-(h_p\sin\theta)^2}\right] \times \sqrt{1-(h_a\cos\theta)^2}\, h_a \cos\theta \cos\phi, \quad (7)$$

$$P_{[001]} = A_a\left[(h_p\sin\theta)^2 - h_p\sin\theta\sqrt{1-(h_p\sin\theta)^2} - \tfrac{1}{2}\right] \times [1-(h_a\cos\theta)^2]\sin(2\phi). \quad (8)$$

Here, $h_p = H/H^{\rm Sat}_{\rm plane}$ and $h_a = H/H^{\rm Sat}_{\rm axis}$ are the magnitudes of the applied field H in the units of the saturation fields. The θ and ϕ denote the polar and azimuthal angles of the magnetic field relative to the [001] and [100] axes, respectively. A_p and A_a are coefficients describing the strength of the magnetoelectric coupling. To make the formulas more compact, the tilting angle of the two inequivalent oxygen tetrahedra in the unit cell was approximated by $\pi/4$, which is close to the experimental value of 48° for CCSO [21]. For BCGO the saturation fields are $H^{\rm Sat}_{\rm plane} \approx 16$ T and $H^{\rm Sat}_{\rm axis} \approx 36$ T as found in the static [43] and optical experiments [49]. By fitting the field dependence of the static polarization, reproduced from Refs. [18,19] in Figs. 1(a) and 1(g), we obtain $A_{\rm plane} = 410\ \mu{\rm C/m^2}$ and $A_{\rm axis} = 180\ \mu{\rm C/m^2}$ for BCGO. Using these parameters, the field dependence of every component of the static ME tensor $\chi^{em}_{\delta\gamma} = c\partial P_\delta/\partial H_\gamma$ can be calculated for BCGO using Eqs. (6)–(8).

For these three compounds, several elements of the static ME tensor, which are used in the present study for comparison with the directional dichroism spectra, can be directly determined from the measured field dependence of the ferroelectric polarization reported in the literature. Only in those cases when experimental curves are not available, the ME tensor elements are evaluated using the fitted parameters as described above.

Figure 1(a) shows $P_{[001]}$ induced by $H_{[110]}$ (reproduced from Ref. [18]) and the field dependence of the corresponding element of the static ME tensor, $\chi^{em}_{[001],[110]} = c\partial P_{[001]}/\partial H_{[110]}$, is shown in Fig. 1(c). The sum rule, Eq. (5), relates this element of static ME to the directional dichroism spectrum in the Voigt configuration, where the magnetic component of light is parallel to the static magnetic field applied along the [110] direction and the electric component of light is parallel to the [001] axis. The corresponding directional dichroism spectra are obtained by subtracting the red and blue absorption spectra in Fig. 1(b) [10]. The comparison between the static and optical data using Eq. (5) is shown Fig. 1(c).

The rest part of Fig. 1, panels (d)–(l), shows similar analysis for other three elements of the ME tensor in BCGO. In two cases, panels (e), (f), (h), and (i), data for SCSO and CCSO are included as well. The dependence of the ferroelectric polarization on the orientation of the magnetic field is shown in panels (d), (g), and (j), the directional dichroism spectra in panels (e), (h), and (k), while the comparison between the static and optical data is given in panels (f), (i), and (l).

The $P_{[100]}(\theta)$ curve in Fig. 1(g) is reproduced from Ref. [18], where θ is the angle of the magnetic field relative to the [001] axis. Since the tilting of the magnetic field from the [010] direction by a small angle $\delta\theta$ creates a weak transversal field $\delta\mathbf{H} = (0, 0, H\sin\delta\theta)$, for $\mathbf{H} \parallel [010]$ one obtains $\chi^{em}_{[100][001]} = c\partial P_{[100]}/\partial H_{[001]} \approx c(\partial P_{[100]}/\partial\theta)H^{-1}$. The corresponding optical experiment can be realized in the Faraday configuration ($\mathbf{H} \parallel [010]$), while the electric and magnetic components of light are parallel to the [100] and [001] axes, respectively. These THz absorption spectra are shown for the two opposite wave propagation directions in Fig. 1(h) as reproduced from Ref. [11] for BCGO and from Ref. [12] for CCSO.

The $P_{[001]}(\phi)$ curve in Fig. 1(d) is taken from Ref. [18] and the $P_{[110]}(\theta)$ curve in Fig. 1(j) is calculated using Eqs. (6)–(8). In the former and later cases, the elements of the static ME tensor are respectively obtained according to $\chi^{em}_{[001][010]} = c\partial P_{[001]}/\partial H_{[010]} \approx c(\partial P_{[001]}/\partial\phi)H^{-1}$ for $\mathbf{H} \parallel [100]$ and $\chi^{em}_{[110][001]} = c\partial P_{[110]}/\partial H_{[001]} \approx c(\partial P_{[110]}/\partial\theta)H^{-1}$ for $\mathbf{H} \parallel [110]$. The corresponding terahertz absorption spectra are shown in panels (e) and (k), respectively.

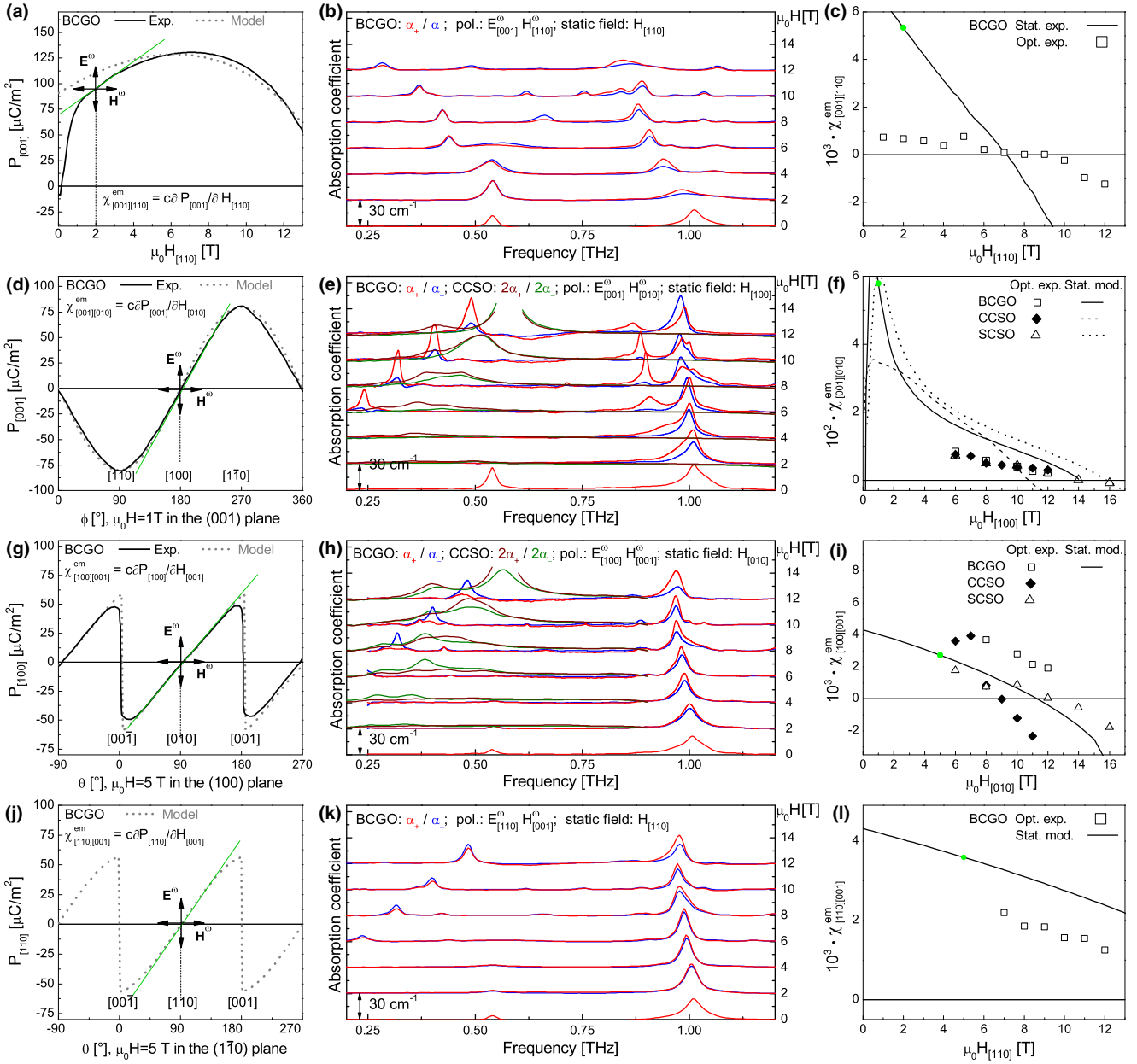

FIG. 1. (Color online) Comparison of the static and optical ME properties of multiferroic $Ba_2CoGe_2O_7$ (BCGO), $Ca_2CoSi_2O_7$ (CCSO) and $Sr_2CoSi_2O_7$ (SCSO) based on the ME sum rule in Eq. (5). (a) Dependence of the ferroelectric polarization (P) on the magnitude of the magnetic field (H) in BCGO. (d), (g), and (j) Dependence of P on the orientation of the field in BCGO. In these panels, the solid lines are experimental data reproduced from Ref. [18], while the dashed lines are calculated using the spin dependent p-d hybridization model according to Eqs. (6)–(8) [18]. The slopes of the green lines in the same panels are proportional to the corresponding elements of the ME tensor. Arrows labeled with $\mathbf{E}^{\omega}$ and $\mathbf{H}^{\omega}$ show the electric and magnetic components of the absorbed light in the corresponding optical experiment, respectively. (b), (e), (h), and (k) Field dependence of the magnon absorption spectra of BCGO in the GHz-THz range. The light polarizations indicated in these panels correspond to the labels $\mathbf{E}^{\omega}$ and $\mathbf{H}^{\omega}$ shown in the panels of the first column. The spectra are shifted vertically proportional to H. For BCGO, the spectra corresponding to counter-propagating light beams are plotted by red and blue lines, while for CCSO brown and dark green lines represent the two propagation directions. The absorption coefficient of CCSO is multiplied by a factor of two for better visibility. The spectra in (b) and (k) are measured in the present study, while the data in (e) and (h) are reproduced from Ref. [11] for BCGO and from Ref. [12] for CCSO, respectively. (c), (f), (i), and (l) Magnetic field dependence of different components of the ME tensor. Symbols indicate the tensor elements calculated from the corresponding optical measurements using the ME sum rule; empty square, full diamond and empty triangle stand for BCGO, CCSO, and SCSO, respectively. The field dependence of the static ME tensor components are plotted with solid, dashed and dotted lines for the three compounds in the same order. The points corresponding to the slope of the green lines in the left panels are indicated by a green dot. The solid line in (c) is calculated directly from the measured polarization-magnetic field curve shown in (a), while the curves in (f), (i), and (l) are evaluated using Eqs. (6)–(8). Static experiments, optical measurements, and model calculations were carried out at $T = 2$, 4, and 0 K, respectively.

III. DISCUSSION

The comparison between the ME tensor elements calculated from the static and optical data in the last column of Fig. 1 supports the applicability of the ME sum rule in these multiferroic compounds. The magnitude and the field dependence of the static and optical data in panels (f), (i), and (l) show quantitative agreement. Their difference can be attributed to the following factors: (i) the directional dichroism measurements were performed at $T = 4$ K, while the static experiments were carried out at $T \leqslant 2$ K where the ME coefficients are larger by ~10%–20%, (ii) the two set of experiments were performed on samples from different growths, (iii) in Figs. 1(e) and 1(h), the polarization of light beams can change during the propagation through the samples due to natural and magnetic circular dichroism, (iv) the model, Eqs. (6)–(8), used to calculate the field dependence of the static ME coefficients is not accurate because the assumed linear field dependence of the magnetization does not hold, and (v) uncertainty in the geometrical factors of samples used in the static and optical experiments may also cause an error of typically 10%–20%.

In the last three rows of Fig. 1, the dominant contribution to the integral in the ME sum rule comes from the Goldstone mode. This mode has a small resonance frequency of less than 0.075 THz in zero field and becomes gapped in proportion to the easy-plane component of the static magnetic field [49]. In the field region investigated here, its energy remains considerably smaller than those of the other magnon modes. Hence it dominates the integral in Eq. (5) sum rule due to the ω^2 frequency denominator. This mode is not excited in an easy-plane magnet if the magnetic component of light is parallel to the static magnetic field as seen in Fig. 1(b). Correspondingly, in Fig. 1(c), the ME tensor element calculated from the directional dichroism data is smaller than in the other three cases, (f), (i), and (l), where the Goldstone mode is excited.

The ME tensor element calculated from the sum rule in Fig. 1(c) is one order of magnitude smaller than the value determined from the static measurement, though they both change sign at about 7 T. This significant difference may come from directional dichroism exhibited by excitations out of range of our optical detection. These additional modes cannot be spin wave modes because all the six magnon modes theoretically predicted for an $S = 3/2$ easy-plane antiferromagnet have been observed below 1.5 THz, the frequency window of the current study [49]. As another possibility, the dynamics of ME domain walls could also contribute to the static ME susceptibility. However, the presence of such ME domain-wall dynamics should be restricted to the region of $B < 1$ T, when the field is applied within the easy-plane, since the single-domain multiferroic state is realized in higher fields for these compounds [18,43]. Therefore we think that the optical modes contributing to the static ME effect could be low-energy phonon modes hybridized with the magnon modes. Though directional dichroism has not been directly observed for phonon modes, recent optical studies on multiferroic $Ba_3NbFe_3Si_2O_{14}$ reported about the magnetoelectric nature of low-energy lattice vibrations [51].

Besides the comparative analysis of static and optical ME data carried out for the three compounds above to demonstrate the applicability of the ME sum rule, we also make predictions for the same and other multiferroic materials. Previous studies report magnetically induced ferroelectric polarization in the paramagnetic phase of BCGO [19] and SCSO [16,17] up to $T = 300$ K, although their magnetic ordering temperature is below 10 K. Since the magnetic symmetry (MPG) of these compounds is the same for the ordered and the paramagnetic state, we expect that the directional dichroism observed below T_N in various configurations survives up to room temperature.

In the noncentrosymmetric soft magnet $(Cu,Ni)B_2O_4$, the electric control of the magnetization direction has been demonstrated together with directional dichroism of near-infrared electronic d-d excitations [52]. The contribution from these d-d transitions to the ME sum rule is negligible due to their high frequency and the ω^2 denominator in Eq. (5), thus we expect that the directional dichroism should also be present for low-frequency magnon excitations in this material.

The magnetic control of the ferroelectric polarization and/or the electric control of the magnetization have been observed in a plethora of multiferroic materials including perovskite manganites with cycloidal spin order [53–56], the room temperature multiferroics $BiFeO_3$ [57,58] and $Sr_3Co_2Fe_{24}O_{41}$ [59,60]. Based on the ME sum rule, we predict that these compounds should also show directional dichroism as already has been found in $Eu_{0.55}Y_{0.45}MnO_3$ [13] and $Gd_{0.5}Tb_{0.5}MnO_3$ [14] in the spectral range of the magnon excitations.

IV. CONCLUSIONS

We derived a magnetoelectric (ME) sum rule and discussed its validity for a broad class of materials simultaneously lacking the spatial inversion and the time reversal symmetries. We showed that the ME sum rule can be used to predict the static ME properties based on the directional dichroism spectra governed by the optical ME effect and vica versa. We verified this approach by a quantitative comparison between static ME coefficients and directional dichroism spectra experimentally determined for three multiferroic compounds in the melilite family. In most cases we found that the dominant contribution to the ME sum rule comes from the magnon excitations in the GHz-THz region. Our approach is applicable to most of the ME multiferroics where the magnetically induced electric polarization can be controlled by the magnitude or the direction of external magnetic field.

ACKNOWLEDGMENTS

We thank Y. Tokura, H. Murakawa and K. Penc for valuable discussions. This project was supported by Hungarian Research Funds OTKA K108918, TÁMOP-4.2.2.B-10/1-2010-0009, TÁMOP-4.2.1/B-09/1/KMR-2010-0002, TÁMOP 4.2.4. A/2-11-1-2012-0001, by the Estonian Ministry of Education and Research under Grants SF0690029s09 and IUT23-03, by the Estonian Science Foundation under Grants ETF8170 and ETF8703 and by the bilateral program of the Estonian and Hungarian Academies of Sciences under the Contract No. SNK-64/2013. S.B. was supported by the Funding Program for World-Leading Innovative R&D on Science and Technology (FIRST Program), Japan.

APPENDIX A: OPTICAL MEASUREMENT OF MAGNETOELECTRIC TENSOR ELEMENTS IN CHIRAL MATERIALS

Following Ref. [12], we consider the highest symmetry when magneto-chiral dichroism can be observed in crystals, namely the chiral magnetic point group $42'2'$. When the light propagates parallel to the fourfold axis (chosen as the z axis), there are four different indices of refraction corresponding the two opposite propagation directions ($\pm$) and the two circular polarizations (l/r):

$$N^l_\pm = \sqrt{(\varepsilon'_{xx} \mp i\varepsilon''_{yx})(\mu'_{xx} \mp i\mu''_{yx})} + i\chi^{me\,\prime\prime}_{xx} \pm \chi^{me\,\prime}_{yx}, \quad \text{(A1)}$$

$$N^r_\pm = \sqrt{(\varepsilon'_{xx} \pm i\varepsilon''_{yx})(\mu'_{xx} \pm i\mu''_{yx})} - i\chi^{me\,\prime\prime}_{xx} \pm \chi^{me\,\prime}_{yx}. \quad \text{(A2)}$$

Here primes and double primes respectively denote the time reversal even and odd parts of the dielectric permittivity and magnetic permeability tensor elements. The assignment is opposite for the ME tensor, i.e., prime and double prime denote the time-reversal odd and even parts, respectively. Using all the four indices of refraction, the time-reversal odd $\chi^{me\,\prime}_{yx}$ tensor element can be expressed as

$$\chi^{me\,\prime}_{yx} = \frac{(N^l_+ - N^l_-) + (N^r_+ - N^r_-)}{4}. \quad \text{(A3)}$$

Thus $\Im\chi^{me\,\prime}_{yx}$ can be experimentally determined by measuring the directional dichroism spectra for circularly polarized beams. $\Im\chi^{me\,\prime}_{yx}$ can also be obtained when using a linearly polarized incident beam and a polarization-independent detection scheme. In this case, neglecting the reflection losses, the transmitted intensity reads as

$$\begin{aligned} I_\pm &= \frac{I_0}{2}(e^{-\alpha^l_\pm d} + e^{-\alpha^r_\pm d}) \\ &= I_0 e^{-\frac{\alpha^l_\pm + \alpha^r_\pm}{2} d} \mathrm{ch}\left(\frac{\alpha^l_\pm - \alpha^r_\pm}{2} d\right) \end{aligned} \quad \text{(A4)}$$

independently from the polarization plane of the incoming wave. Here, I_0 is the incoming intensity and d is the thickness of the sample. For linearly polarized incident beams one can define an effective directional absorption difference $\Delta\alpha_{\mathrm{eff}} = -\ln(I_+/I_-)/d$. Keeping only terms that are of first order in the ME response:

$$\begin{aligned} \Delta\alpha_{\mathrm{eff}} \approx{}& \frac{4\omega}{c}\Im\chi^{me\,\prime}_{yx} + d\left(\frac{2\omega}{c}\right)^2 \Re\chi^{me\,\prime\prime}_{xx} \\ &\times \Re\left[\sqrt{\varepsilon'_{xx}\mu'_{xx}}\left(\frac{\varepsilon''_{yx}}{\varepsilon'_{xx}} + \frac{\mu''_{yx}}{\mu'_{xx}}\right)\right]. \end{aligned} \quad \text{(A5)}$$

The thickness-dependent second term corresponds to the cascade effect of the natural and magnetic circular dichroisms. As it was shown the contribution of the second term to the absorption difference in chiral crystals is negligibly small compared to the contribution of the first $\Im\chi^{me\,\prime}_{yx}$ term [61]. This is due to the fact that the diagonal elements of the dielectric permittivity and the magnetic permeability tensors are usually much larger than the off-diagonal ones.

APPENDIX B: DERIVATION OF THE MAGNETOELECTRIC SUM RULE FROM THE KUBO FORMULA

The linear response of a quantum system to external stimuli is given by the Kubo formula. The frequency dependent ME susceptibility tensor at the finite temperatures reads as

$$\begin{aligned} \chi^{me}_{\gamma\delta}(z) = -\frac{V_c}{\hbar}\sqrt{\frac{\mu_0}{\varepsilon_0}}\sum_{m,n}\frac{e^{-\beta\hbar\omega_n} - e^{-\beta\hbar\omega_m}}{\sum_i e^{-\beta\hbar\omega_i}} \\ \times \frac{\langle n|M_\gamma|m\rangle\langle m|P_\delta|n\rangle}{z - \omega_m + \omega_n}, \end{aligned} \quad \text{(B1)}$$

where $z = \omega + i\varepsilon$ and $\varepsilon \to 0+$. M_γ and P_δ are the operators of the magnetic and electric dipole density, respectively. $|m\rangle$ and $|n\rangle$ are the eigenstates of the system with energies of $\hbar\omega_m$ and $\hbar\omega_n$; β is the inverse temperature and V_c stands for the volume of the unit cell. In the zero-temperature limit, the Boltzmann factors vanish except for the ground state $|0\rangle$. Using the relation $\lim_{\varepsilon\to 0}\frac{1}{x+i\varepsilon} \equiv \mathcal{P}\frac{1}{x} - i\pi\delta(x)$, the real and imaginary parts of $\chi^{me}_{\gamma\delta}(\omega)$ can be separated:

$$\begin{aligned} \Re\chi^{me}_{\gamma\delta}(\omega) = -\frac{V_c}{\hbar}\sqrt{\frac{\mu_0}{\varepsilon_0}}\sum_m \Bigg\{ & \mathcal{P}\frac{2\omega_m \Re(\langle 0|M_\gamma|m\rangle\langle m|P_\delta|0\rangle)}{\omega^2 - \omega_m^2} \\ & + \pi\Im(\langle 0|\,M_\gamma\,|m\rangle\,\langle m|\,P_\delta\,|0\rangle)[\delta(\omega - \omega_m) \\ & - \delta(\omega + \omega_m)]\Bigg\}, \end{aligned} \quad \text{(B2)}$$

$$\begin{aligned} \Im\chi^{me}_{\gamma\delta}(\omega) = -\frac{V_c}{\hbar}\sqrt{\frac{\mu_0}{\varepsilon_0}}\sum_m \Bigg\{ & \mathcal{P}\frac{2\omega \Im(\langle 0|M_\gamma|m\rangle\langle m|P_\delta|0\rangle)}{\omega^2 - \omega_m^2} \\ & - \pi\Re(\langle 0|M_\gamma|m\rangle\langle m|P_\delta|0\rangle)[\delta(\omega - \omega_m) \\ & - \delta(\omega + \omega_m)]\Bigg\}. \end{aligned} \quad \text{(B3)}$$

These expressions can also be obtained by the second order perturbation theory [24]. The real/imaginary part of the transition matrix element product is antisymmetric/symmetric under time reversal because time reversal changes the sign of the magnetic dipole operator and also requires the conjugation of the matrix elements due to the exchange of the initial and final states. As it is obvious from Eq. (B2), the imaginary part of the matrix element products does not contribute to the static ME susceptibility. Using Eq. (4), one can reproduce the ME sum rule:

$$\begin{aligned} \chi^{me}_{\gamma\delta}(0) &= \frac{2V_c}{\hbar}\sqrt{\frac{\mu_0}{\varepsilon_0}}\sum_m \frac{\Re(\langle 0|M_\gamma|m\rangle\langle m|P_\delta|0\rangle)}{\omega_m} \\ &= \frac{2V_c}{\hbar}\sqrt{\frac{\mu_0}{\varepsilon_0}}\sum_m \Re\langle 0|M_\gamma|m\rangle\langle m|P_\delta|0\rangle \\ &\quad \times \int_0^\infty \frac{\delta(\omega - \omega_m) - \delta(\omega + \omega_m}{\omega}\mathrm{d}\omega \\ &= \frac{c}{2\pi}\mathcal{P}\int_0^\infty \frac{\Delta\alpha(\omega)}{\omega^2}\mathrm{d}\omega. \end{aligned} \quad \text{(B4)}$$

In the derivation above, we used Eqs. (B2) and (B3) and the identities $\int_0^\infty \frac{\delta(\omega+\omega_m)}{\omega}\mathrm{d}\omega = 0$ and $\mathcal{P}\int_0^\infty \frac{1}{\omega^2-\omega_m^2}\mathrm{d}\omega = 0$. From the derivation above, it is also obvious that the time-reversal

even (imaginary) part of the ME tensor does not contribute to the frequency integral in Eq. (1), thus, $\Im\chi^{me}_{\gamma\delta}(\omega)$ we can be replaced by $\frac{c}{2\omega}\Delta\alpha(\omega) = \Im(\chi^{me}_{\gamma\delta}(\omega) - \{\chi^{me}_{\gamma\delta}(\omega)\}')$ in the ME sum rule.

[1] *Magnetoelectric Interaction Phenomena in Crystals*, edited by A. J. Freeman and H. Schmid (Gordon and Breach, London, 1995).
[2] M. Fiebig, J. Phys. D: Appl. Phys. **38**, R123 (2005).
[3] W. Eerenstein, N. D. Mathur, and J. F. Scott, Nature (London) **442**, 759 (2006).
[4] R. Ramesh and N. A. Spaldin, Nat. Mater. **6**, 21 (2007).
[5] L. W. Martin, Y.-H. Chuc, and R. Ramesh, Mater. Sci. Eng. R **68**, 89 (2010).
[6] S. M. Wu, Shane A. Cybart, D. Yi, James M. Parker, R. Ramesh, and R. C. Dynes, Phys. Rev. Lett. **110**, 067202 (2013).
[7] A. Pimenov, A. A. Mukhin, V. Y. Ivanov, V. D. Travkin, A. M. Balbashov, and A. Loidl, Nat. Phys. **2**, 97 (2006).
[8] A. B. Sushkov, R. V. Aguilar, S. Park, S. W. Cheong, and H. D. Drew, Phys. Rev. Lett. **98**, 027202 (2007).
[9] P. Rovillain, R. De Sousa, Y. T. Gallais, A. Sacuto, M. A. Méasson, D. Colson, A. Forget, M. Bibes, A. Barthélémy, and M. Cazayous, Nat. Mater. **9**, 975 (2010).
[10] I. Kézsmárki, N. Kida, H. Murakawa, S. Bordács, Y. Onose, and Y. Tokura, Phys. Rev. Lett. **106**, 057403 (2011).
[11] S. Bordács, I. Kézsmárki, D. Szaller, L. Demkó, N. Kida, H. Murakawa, Y. Onose, R. Shimano, T. Rõõm, U. Nagel, S. Miyahara, N. Furukawa, and Y. Tokura, Nat. Phys. **8**, 734 (2012).
[12] I. Kézsmárki, D. Szaller, S. Bordács, V. Kocsis, Y. Tokunaga, Y. Taguchi, H. Murakawa, Y. Tokura, H. Engelkamp, T. Rõõm, and U. Nagel, Nat. Commun. **5**, 3203 (2014).
[13] Y. Takahashi, R. Shimano, Y. Kaneko, H. Murakawa, and Y. Tokura, Nat. Phys. **8**, 121 (2012).
[14] Y. Takahashi, Y. Yamasaki, and Y. Tokura, Phys. Rev. Lett. **111**, 037204 (2013).
[15] A. Shuvaev, V. Dziom, Anna Pimenov, M. Schiebl, A. A. Mukhin, A. C. Komarek, T. Finger, M. Braden, and A. Pimenov, Phys. Rev. Lett. **111**, 227201 (2013).
[16] M. Akaki, H. Iwamoto, T. Kihara, M. Tokunaga, and H. Kuwahara, Phys. Rev. B **86**, 060413(R) (2012).
[17] M. Akaki, T. Tadokoro, T. Kihara, M. Tokunaga, and H. Kuwahara, J. Low Temp. Phys. **170**, 291 (2013).
[18] H. Murakawa, Y. Onose, S. Miyahara, N. Furukawa, and Y. Tokura, Phys. Rev. Lett. **105**, 137202 (2010).
[19] H. Murakawa, Y. Onose, S. Miyahara, N. Furukawa, and Y. Tokura, Phys. Rev. B **85**, 174106 (2012).
[20] M. Akaki, J. Tozawa, D. Akahoshi, and H. Kuwahara, Appl. Phys. Lett. **94**, 212904 (2009).
[21] K. Kusaka, K. Hagiya, M. Ohmasa, Y. Okano, M. Mukai, K. Iishi, and N. Haga, Phys. Chem. Miner. **28**, 150 (2001).
[22] Y. Yamada and G. Shirane, J. Phys. Soc. Jpn. **26**, 396 (1969).
[23] S. Kamba, D. Nuzhnyy, P. Vaněk, M. Savinov, K. Knížek, Z. Shen, E. Šantavá, K. Maca, M. Sadowski, and J. Petzelt, Europhys. Lett. **80**, 27002 (2007).
[24] L. D. Barron, *Molecular Light Scattering and Optical Activity* (Cambridge University Press, Cambridge, 2004).
[25] N. Berova, K. Nakanishi, and R. W. Woody, *Circular Dichroism: Principles and Applications*, 2nd ed. (Wiley-VCH, Berlin, 2000).
[26] D. Szaller, S. Bordács, and I. Kézsmárki, Phys. Rev. B **87**, 014421 (2013).
[27] R. M. Hornreich and S. Shtrikman, Phys. Rev. **171**, 1065 (1968).
[28] T. H. O'Dell, *The Electrodynamics of Magnetoelectric Media* (North-Holland, Amsterdam, 1970).
[29] T. Arima, J. Phys.: Condens. Matter. **20**, 434211 (2008).
[30] A. Cano, Phys. Rev. B **80**, 180416(R) (2009).
[31] N. A. Spaldin, M. Fiebig, and M. Mostovoy, J. Phys.: Condens. Matter **20**, 434203 (2008).
[32] S. Miyahara and N. Furukawa, J. Phys. Soc. Jpn. **80**, 073708 (2011).
[33] S. Miyahara and N. Furukawa, J. Phys. Soc. Jpn. **81**, 023712 (2012).
[34] J.-P. Rivera, Eur. Phys. J. B **71**, 299 (2009).
[35] R. Resta, Phys. Rev. Lett. **106**, 047202 (2011).
[36] K. Hagiya, M. Ohmasa, and K. Iishi, Acta Cryst. **B49**, 172 (1993).
[37] Z. H. Jia, A. K. Schaper, W. Massa, W. Treutmann, and H. Rager, Acta Cryst. **B62**, 547 (2006).
[38] A. Zheludev, T. Sato, T. Masuda, K. Uchinokura, G. Shirane, and B. Roessli, Phys. Rev. B **68**, 024428 (2003).
[39] V. Hutanu, A. Sazonov, H. Murakawa, Y. Tokura, B. Náfrádi, and D. Chernyshov, Phys. Rev. B **84**, 212101 (2011)
[40] M. Akaki, J. Tozawa, D. Akahoshi, and H. Kuwahara, J. Phys.: Conf. Ser. **150**, 042001 (2009).
[41] T. Sato, T. Masuda, and K. Uchinokura, Phys. B **329–333**, 880 (2003).
[42] V. Hutanu, A. Sazonov, M. Meven, H. Murakawa, Y. Tokura, S. Bordács, I. Kézsmárki, and B. Náfrádi, Phys. Rev. B **86**, 104401 (2012).
[43] V. Hutanu, A. P. Sazonov, M. Meven, G. Roth, A. Gukasov, H. Murakawa, Y. Tokura, D. Szaller, S. Bordács, I. Kézsmárki, V. K. Guduru, L. C. J. M. Peters, U. Zeitler, J. Romhányi, and B. Náfrádi, Phys. Rev. B **89**, 064403 (2014).
[44] K. Yamauchi, P. Barone, and S. Picozzi, Phys. Rev. B **84**, 165137 (2011).
[45] J. M. Perez-Mato, and J. L. Ribeiro, Acta Cryst. A **67**, 264 (2011).
[46] P. Toledano, D. D. Khalyavin, and L. C. Chapon, Phys. Rev. B **84**, 094421 (2011).
[47] H. T. Yi, Y. J. Choi, S. Lee, and S. W. Cheong, Appl. Phys. Lett. **92**, 212904 (2008)
[48] M. Matsumoto, M. Soda, and T. Masuda, J. Phys. Soc. Jpn. **82**, 093703 (2013).
[49] K. Penc, J. Romhányi, T. Rõõm, U. Nagel, Á. Antal, T. Fehér, A. Jánossy, H. Engelkamp, H. Murakawa, Y. Tokura, D. Szaller, S. Bordács, and I. Kézsmárki, Phys. Rev. Lett. **108**, 257203 (2012).
[50] T. Arima, J. Phys. Soc. Jpn. **76**, 073702 (2007).
[51] L. Chaix, S. de Brion, F. Lévy-Bertrand, V. Simonet, R. Ballou, B. Canals, P. Lejay, J. B. Brubach, G. Creff, F. Willaert, P. Roy, and A. Cano, Phys. Rev. Lett. **110**, 157208 (2013).
[52] M. Saito, K. Ishikawa, S. Konno, K. Taniguchi, and T. Arima, Nat. Mat. **8**, 634 (2009).

[53] Xiaoyan Yao and Qichang Li, Europhys. Lett. **88**, 47002 (2009).
[54] Xiaoyan Yao, J. Phys. Soc. Jpn. **79**, 043801 (2010).
[55] T. Kimura, T. Goto, H. Shintani, K. Ishizaka, T. Arima, and Y. Tokura, Nature (London) **426**, 55 (2003).
[56] H. Murakawa, Y. Onose, F. Kagawa, S. Ishiwata, Y. Kaneko, and Y. Tokura, Phys. Rev. Lett. **101**, 197207 (2008).
[57] T. Zhao, A. Scholl, F. Zavaliche, K. Lee, M. Barry, A. Doran, M. P. Cruz, Y. H. Chu, C. Ederer, N. A. Spaldin, R. R. Das, D. M. Kim, S. H. Baek, C. B. Eom, and R. Ramesh, Nat. Mater. **5**, 823 (2006).
[58] Seoungsu Lee, W. Ratcliff, S. W. Cheong, and V. Kiryukhin, Appl. Phys. Lett. **92**, 192906 (2008).
[59] Y. Kitagawa, Y. Hiraoka, T. Honda, T. Ishikura, H. Nakamura, and T. Kimura, Nat. Mater. **9**, 797 (2010).
[60] S. H. Chun, Y. S. Chai, B.-G. Jeon, H. J. Kim, Y. S. Oh, I. Kim, H. Kim, B. J. Jeon, S. Y. Haam, J.-Y. Park, S. H. Lee, J.-H. Chung, J.-H. Park, and K. H. Kim, Phys. Rev. Lett. **108**, 177201 (2012).
[61] G. L. J. A. Rikken and E. Raupach, Phys. Rev. E **58**, 5081 (1998).